Supplementary Information

High-performance all-solid-state electrolyte for sodium batteries enabled by the interaction between the anion in salt and Na_3SbS_4

Yong Lu[+], *Lin Li*[+], *Qiu Zhang, Yichao Cai, Youxuan Ni, and Jun Chen**

Frontiers Science Center for New Organic Matter, Renewable Energy Conversion and Storage Center (RECAST), Haihe Laboratory of Sustainable Chemical Transformations, Key Laboratory of Advanced Energy Materials Chemistry (Ministry of Education), College of Chemistry, Nankai University, Tianjin 300071, China

[+]These authors contributed equally to this work.

[*]Correspondence: chenabc@nankai.edu.cn

Supplementary Information contains this PDF file and one Video file ("Supplementary Video S1.mp4").

Table of Contents

Experimental Section

Synthesis of Na_3SbS_4

Na_3SbS_4 was synthesized according to the previous literature.[1] In a typical synthesis, 12 mmol (0.936 g) anhydrous Na_2S (Aladdin, Shanghai, China), 4 mmol (0.128 g) S (Aladdin, Shanghai, China), and 2 mmol (0.583 g) Sb_2O_3 (Aladdin, Shanghai, China) were added to 4 mL H_2O at 50 °C in turn. Then, the mixture was stirred at 60 °C for 30 mins, followed by filtration. The filtrate was put in ice bath for 1 h and then filtered to get precipitate. The precipitate was crystalized again to obtain pure Na_3SbS_4 sample. The sample was dried under vacuum at 80 °C for 12 h and then 150 °C for 6 h. Before preparing all-solid-state electrolytes, the sample was ball-milled (weight ratio of sample to bead is 1:20) at 500 rpm for 6 h under Ar atmosphere and stored in an Ar-filled glove box where O_2 and H_2O concentrations were kept less than 0.1 ppm. The reactions during synthesis can be described as:

$$6\ Na_2S + 2\ S + Sb_2O_3 + 21\ H_2O = 2\ Na_3SbS_4 \cdot 9H_2O + 6\ NaOH \quad (1)$$

$$Na_3SbS_4 \cdot 9H_2O \triangleq Na_3SbS_4 + 9\ H_2O \quad (2)$$

Preparation of all-solid-state electrolyte

The all-solid-state electrolyte was prepared via a simple solution casting method. For the preparation of PEO/NaTFSI electrolyte, PEO (1 g, molecular weight: 600000, Aladdin, Shanghai, China) and NaTFSI (0.689 g, molar ratio of EO to Na^+ is 10:1, DodoChem, Suzhou, China) were added to anhydrous acetonitrile (HEOWNS, Tianjin, China, treated with activated 3Å molecular sieve to remove trace H_2O before use and stored in an Ar-filled glove box where O_2 and H_2O concentrations were kept less than 0.1 ppm) and stirred intensely for 12 h at room temperature to form homogeneous solution. Then, the solution was poured into a polytetrafluoroethylene mold. The electrolyte film can be obtained after the mold was heated at 65 °C under vacuum for 24 h to remove residual acetonitrile. For the preparation of PEO/NaTFSI/Na_3SbS_4 electrolyte with different contents of Na_3SbS_4, 0.1, 0.15, 0.2, 0.25, 0.3, or 0.4 g Na_3SbS_4 (weight ratio to PEO is 10,

15, 20, 25, 30, or 40 wt%, respectively) was added in the mixture of PEO and NaTFSI before stirring. Other preparation processes are the same as those for the preparation of PEO/NaTFSI electrolyte. To avoid any interference from H_2O, all the electrolyte preparation procedures were conducted in an Ar-filled glove box where O_2 and H_2O concentrations were kept less than 0.1 ppm.

Materials characterizations

The crystal structure of Na_3SbS_4 and the crystallinity of PEO were characterized by X-ray powder diffraction (XRD, Rigaku MiniFlex600, CuKα radiation). The microstructures of Na_3SbS_4, PEO/NaTFSI/Na_3SbS_4 electrolyte, Na metal, and Na–PTCDA batteries were observed via field-emission scanning electron microscopy (SEM, JEOL JSM-7500F). AFM topography image and Young's modulus mapping were obtained with Peak Force QNM mode (Multimode 8.0, Bruker). The surface elemental information and chemical composition of PEO/Na_3SbS_4, PEO/NaTFSI/Na_3SbS_4 electrolyte and Na electrode after cycles, as well as the solubility of Na_3SbS_4 in PEO were confirmed through X-ray photoelectron spectroscopy (XPS, PerkinElmer PHI 1600 ESCA or Thermo Scientific K-Alpha+). In addition, the solubility of Na_3SbS_4 in PEO was also studied by Fourier transform infrared spectroscopy (IR, Bruker Tensor II Sample Compartment RT-DLaTGS). The chemical bonds in PEO/Na_3SbS_4, PEO/NaTFSI electrolyte, and PEO/NaTFSI/Na_3SbS_4 electrolyte were detected by Raman (Thermo-Fisher Scientific, excitation wavelength, 532 nm). The thermal property/stability of PEO/NaTFSI electrolyte and PEO/NaTFSI/Na_3SbS_4 electrolyte were evaluated via differential scanning calorimeter (NETZSCH, DSC204) and thermogravimetric analyzer (NETZSCH, STA 449F3).

Electrochemical measurements

The 3,4,9,10-perylenetetracarboxylic dianhydride (PTCDA, HEOWNS, Tianjin, China) cathode was prepared by mixing active materials (PTCDA, 50 wt%), conductive carbon materials (Super P, 40 wt%), binder (PVDF, 10 wt%), and *N*-methyl-2-pyrrolidinone as dispersing agent to form a slurry. The slurry was smeared onto an Al foil current collector and dried at 80 °C for 12 h in a

vacuum furnace. The mass loading of PTCDA in each cathode is about 0.3–0.5 mg cm^{-2}. The anode of the batteries is Na foil. The all-solid-state Na–PTCDA batteries and Na|Na symmetric cells are CR2032 coin-type and fabricated using all-solid-state PEO/NaTFSI or PEO/NaTFSI/Na_3SbS_4 electrolyte without a separator or additional liquid electrolyte in an Ar-filled glove box where O_2 and H_2O concentrations were kept less than 0.1 ppm. All the all-solid-state Na–PTCDA batteries and Na|Na symmetric cells were tested at 45 °C (The Na–PTCDA batteries with liquid 1M $NaPF_6$/diglyme electrolyte were tested at room temperature). To achieve favorable electrode/electrolyte interface, all the all-solid-state Na–PTCDA batteries were rested at 70 °C for 6 h before rested and tested at 45 °C. The galvanostatic charge/discharge tests at different rates and the potentiostatic charge tests were performed by Land CT2001A battery instrument. Linear sweep voltammetry in the voltage range of 1–6 V at 0.5 mV s^{-1} and electrochemical impedance spectroscopy in the frequency range of 100k–1 Hz with an amplitude of 5 mV were tested by CHI 660E and CHI 760E electrochemical workstation (ChenHua, Shanghai). The formula to calculate Na^+ transference number (t_+) is shown as follows.

$$t_+ = \frac{I_{ss}(\Delta V - I_0 R_0)}{I_0(\Delta V - I_{ss} R_{ss})} \quad (3)$$

where t_+, I_{ss}, and I_0 are the Na^+ transference number, steady-state current, and initial current, respectively. R_{ss} and R_0 are the resistances at steady state and initial state, respectively. ΔV is the applied constant potential. The criterion for achieving steady state is that the current and resistance do not further change under the constant potential.

Density Functional Theory (DFT) Calculation Details

All the DFT calculations were carried out by using the Vienna Ab Initio Simulation Package (VASP) with the projector augmented wave (PAW) method.[2] The electronic exchange and correlation effects were described by the generalized gradient approximation (GGA) functional parameterized by Perdew-Burke-Ernzerhof (PBE).[3] The plane-wave cutoff energy was set to 450 eV. The convergence criteria of energy and force were set to 10^{-4} eV and 0.02 eV $Å^{-1}$, respectively. The Na_3SbS_4(111) surface was modelled by a 2 × 2 supercell. A vacuum layer of above 20 Å was adopted to avoid the interaction between the periodic slabs. The adsorption energies were obtained as follows:

$E_{ads}(Na) = E(NaTFSI) – E(TFSI) – E(Na)$

$E_{ads}(Na)_{sub} = E(sub + NaTFSI) – E(sub + TFSI) – E(Na)$

$E_{ads}(NaTFSI)_{sub} = E(sub + NaTFSI) – E(sub) – E(NaTFSI)$

where E(Na), E(TFSI), and E(NaTFSI) are the energies of Na, TFSI, and NaTFSI, respectively. E(sub + NaTFSI) and E(sub) are the energies of the Na_3SbS_4 substrates with and without adsorbed NaTFSI, respectively. E(sub + TFSI) is the energy of the Na_3SbS_4 substrates with adsorbed TFSI.

Finite Element Method (FEM) Simulation Details

The pillared electrode was built to simulate the unavoidable microscopic swelling on practical electrode surface (Figure S12).[4] The simulation was performed using the mass transportation laws in concentrated solution which consider the interaction between cations and anions. The simulation temperature is set as 318 K according to the practical operating temperature of batteries in this work.

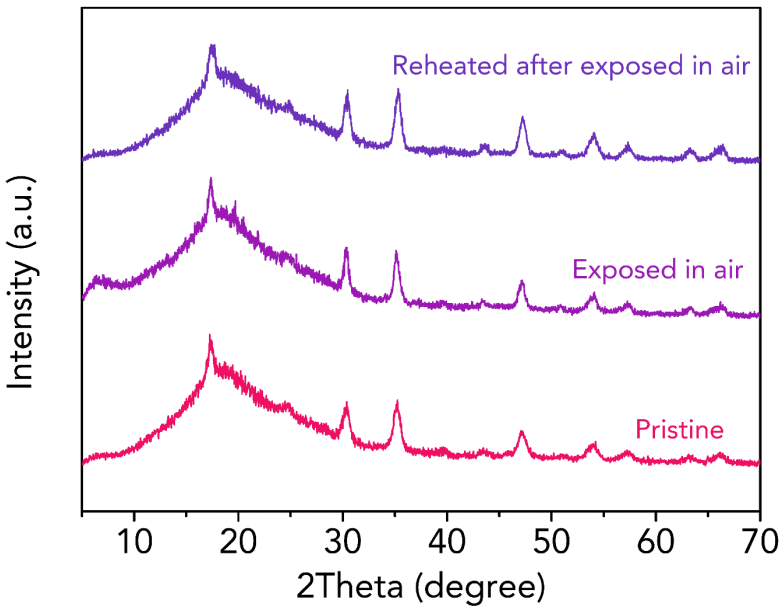

Figure S1. XRD patterns of the prepared Na_3SbS_4 at different states (pristine, exposed in air for 24 h, and reheated at 150 °C under vacuum for 10 h after exposed in air for 24 h).

When testing XRD, we used Kapton film (polyimide) to seal and protect the Na_3SbS_4 sample from contacting with air.

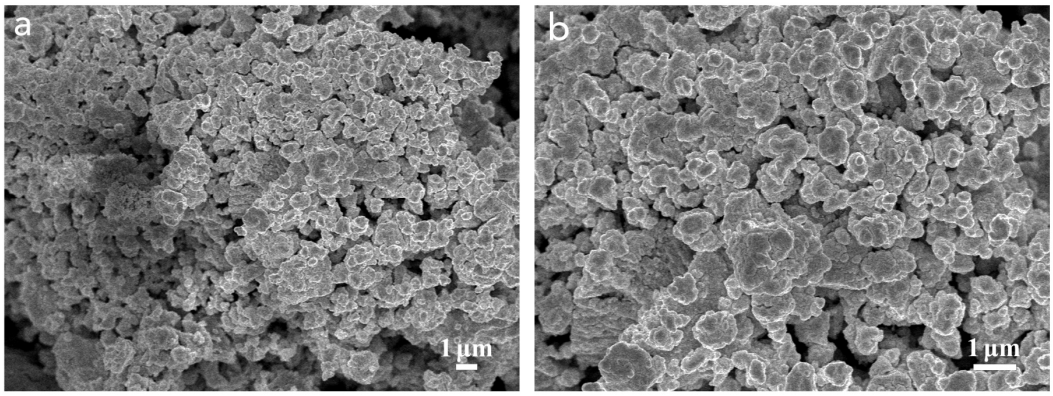

Figure S2. SEM images of the prepared Na_3SbS_4 at (a) low magnification and (b) high magnification.

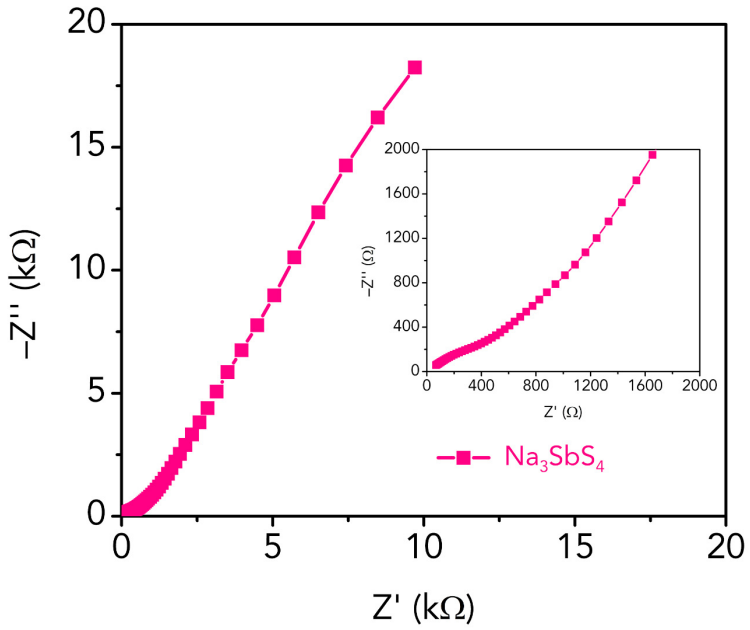

Figure S3. Ionic conductivity of the prepared Na_3SbS_4. Electrochemical impedance spectroscopy (EIS) plot of the Na_3SbS_4 disc with two blocking electrodes (stainless steel) at room temperature. Inset: the enlarged area at the high frequency. The diameter and thickness of the Na_3SbS_4 disc are 16 mm and 1.04 mm, respectively.

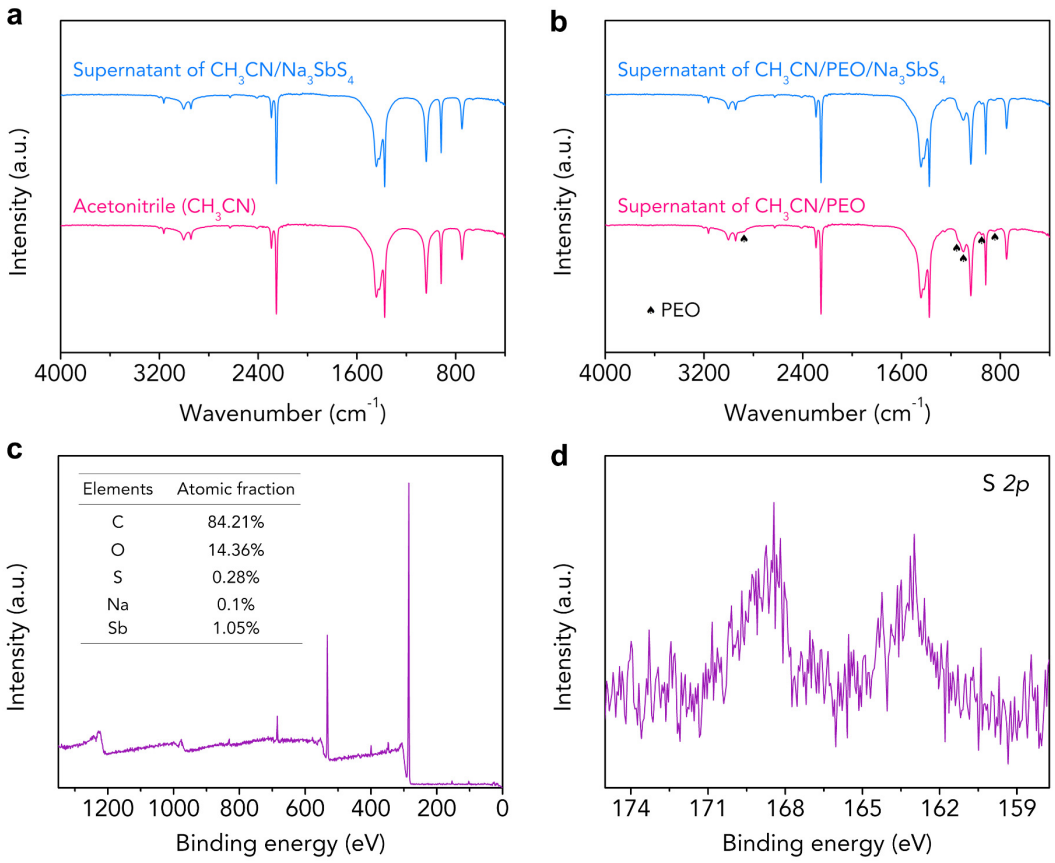

Figure S4. Investigation on whether Na_3SbS_4 can be dissolved in PEO. (a) IR spectra of acetonitrile and the supernatant of acetonitrile/Na_3SbS_4 mixture. (b) IR spectra of the supernatant of acetonitrile/PEO mixture and acetonitrile/PEO/Na_3SbS_4 mixture. (c) XPS survey spectrum and (d) S 2p spectrum of the residual material after removing acetonitrile.

Note that Na_3SbS_4 cannot be dissolved in acetonitrile (Figure S4a) while PEO can be dissolved in acetonitrile (Figure S4b). Thus, we added Na_3SbS_4 into the solution composed of PEO and acetonitrile, and stirred the mixture intensely. Then the mixture was centrifugated, and the obtained supernatant was characterized by IR. As shown in Figure S4b, no signal for Na_3SbS_4 can be detected in the supernatant. We further removed acetonitrile in the supernatant by heating in oven and tested the residual material by XPS. The XPS survey spectrum in Figure S4c and S 2p spectrum in Figure S4d reveal that the S content is extremely low (0.28 at%) and the signal of S is very weak. Both IR and XPS spectra verify that Na_3SbS_4 can be hardly dissolved in PEO. The amounts of Na_3SbS_4, PEO, and acetonitrile in these experiments are 100 mg, 100 mg, and 5 mL, respectively.

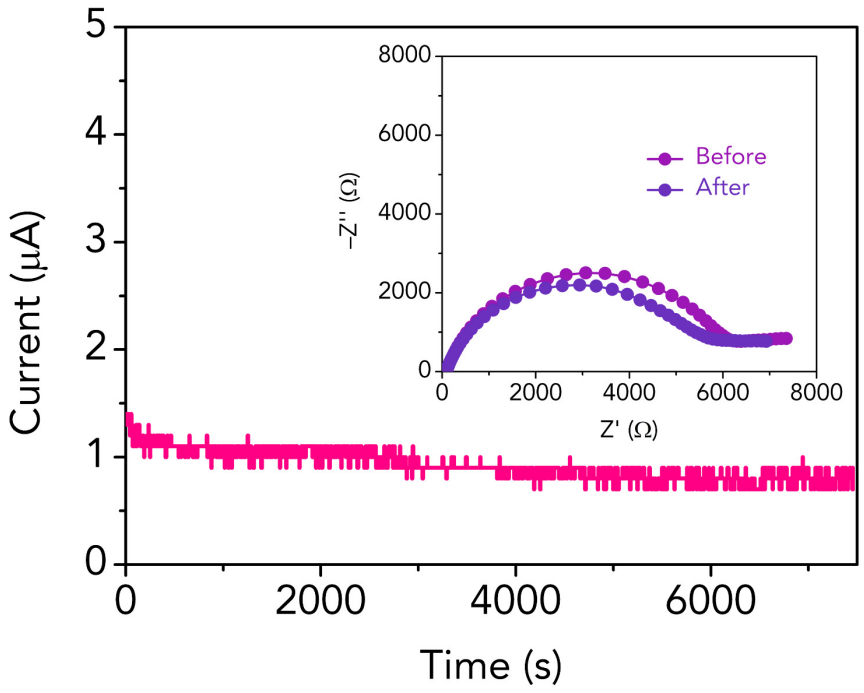

Figure S5. Variation of current with time for the symmetric cell with PEO/NaTFSI electrolyte at an applied voltage of 12 mV. Inset: EIS plots before and after polarization.

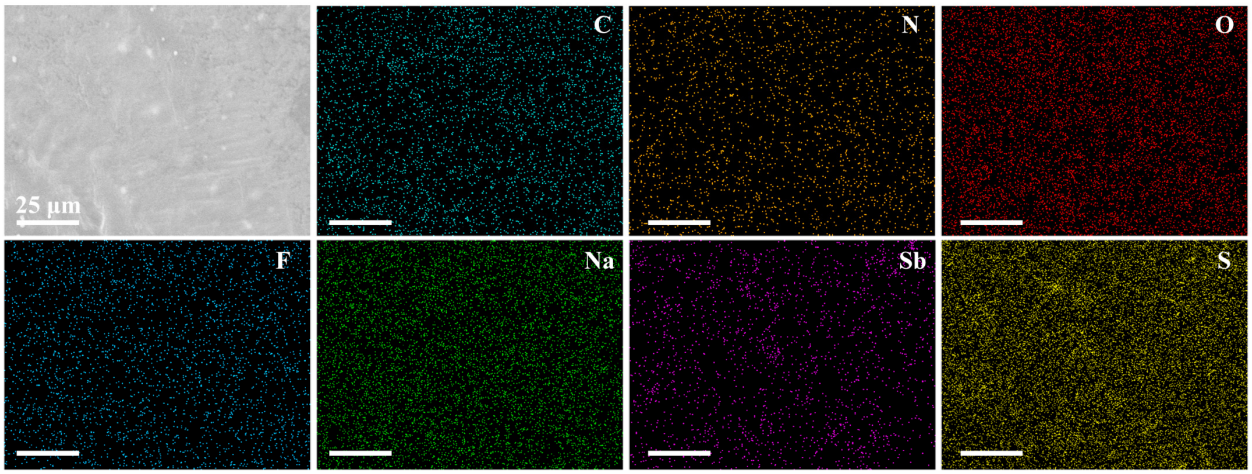

Figure S6. Elemental mapping (C, N, O, F, Na, Sb, and S) of the obtained PEO/NaTFSI/Na_3SbS_4 electrolyte. All the scale bars represent 25 μm.

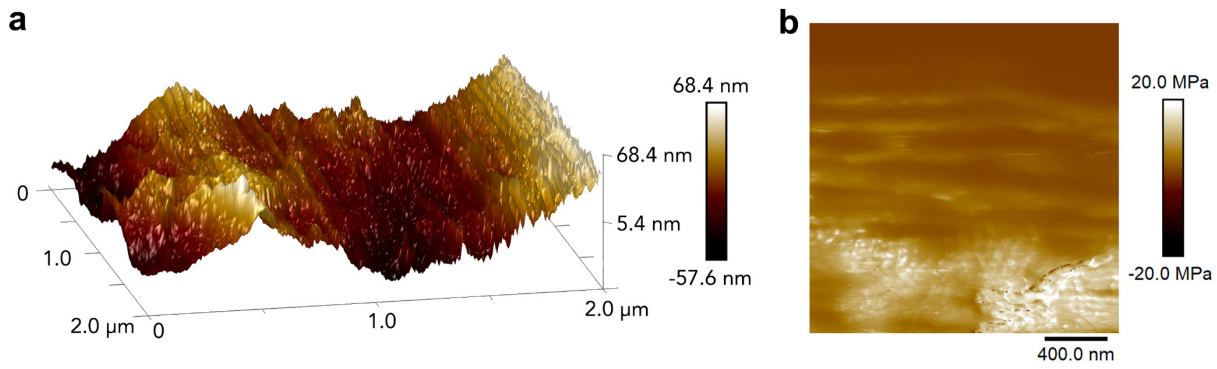

Figure S7. (a) AFM topography image with a 3D view and (b) Young's modulus of the obtained PEO/NaTFSI electrolyte.

Table S1. Comparison on surface roughness and Young's modulus of the PEO/NaTFSI/Na_3SbS_4 electrolyte in this work versus other reported polymer-based all-solid-state electrolytes for sodium batteries.

Electrolyte	Surface roughness (nm)	Young's modulus (MPa)	Ref.
PEO-PVP/$NaPF_6$	130	–	[5]
PMA/PEG/α-Al_2O_3/$NaClO_4$	6	50.79	[6]
PVDF-HFP/SN/$NaClO_4$	–	7.3	[7]
PEO/NaTFSI/Na_3SbS_4	39.3	47.8	This work

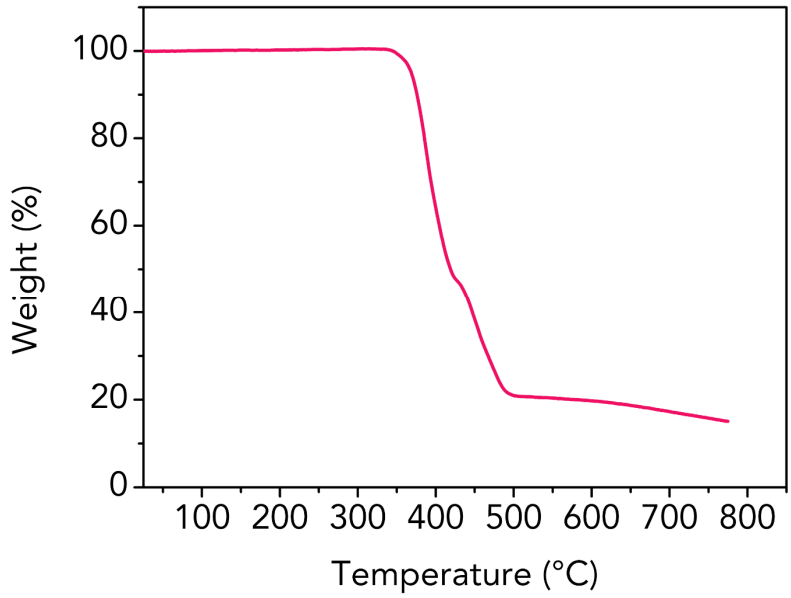

Figure S8. Thermal stability of the PEO/NaTFSI/Na_3SbS_4 electrolyte. TG curve of the electrolyte in the temperature range of 25–775 °C at a heat rate of 5 °C min^{-1} under Ar atmosphere. The weight loss of the electrolyte begins at about 345 °C.

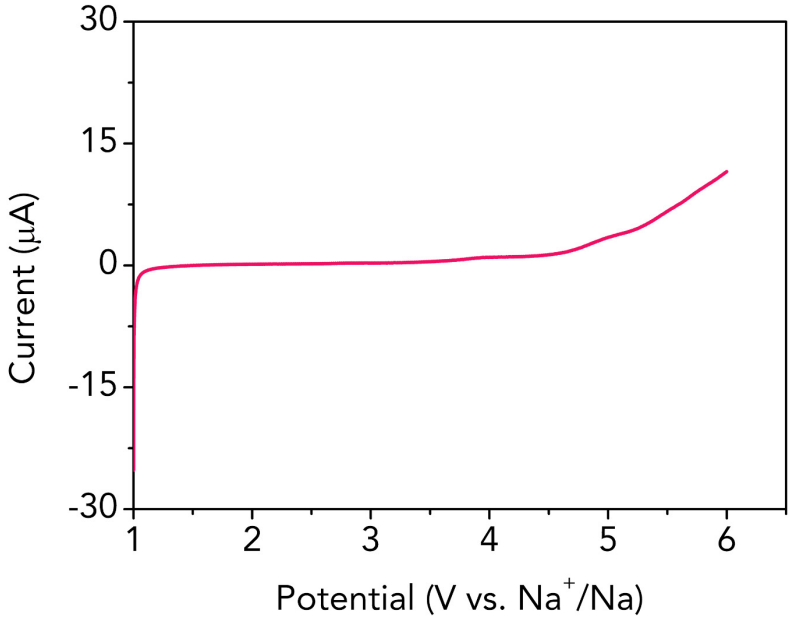

Figure S9. Electrochemical stability window of the PEO/NaTFSI/Na_3SbS_4 electrolyte. Linear sweep voltammetry (LSV) of the electrolyte in the voltage range of 1–6 V at 0.5 mV s^{-1} (45 °C). The anodic decomposition potential of the electrolyte is about 3.7 V (vs. Na^+/Na).

Table S2. Comparison on performance of the PEO/NaTFSI/Na_3SbS_4 electrolyte in this work versus other reported polymer-based all-solid-state electrolytes for sodium batteries.

Electrolyte	Ionic conductivity (S cm^{-1})	Na^+ transference number	Thermal stability (°C)	Ref.
PMA/PEG/α-Al_2O_3/$NaClO_4$	1.46×10^{-4} (70 °C)	–	250	[6]
PEO/NaFNFSI	3.36×10^{-4} (80 °C)	0.24	300	[8]
PEO/CQDs/$NaClO_4$	7.17×10^{-5} (RT)	0.42	–	[9]
PEO/$NaClO_4$/$Na_3Zr_2Si_2PO_{12}$	2.1×10^{-5} (30 °C)	–	–	[10]
CD-HSPE3	2.83×10^{-5} (30 °C) 1.31×10^{-4} (60 °C)	–	280	[11]
POSS-4PEG2K	4.5×10^{-6} (30 °C) 2.6×10^{-4} (80 °C)	–	–	[12]
PEO/E8 LC/$NaIO_4$	1.05×10^{-7} (RT)	0.384	–	[13]
PCL–PTMC:NaFSI	1.64×10^{-5} (25 °C)	0.48	–	[14]
PEO/$NaCF_3SO_3$/MIL-53(Al)	6.87×10^{-5} (60 °C)	0.4	175	[15]
Polyether/NaTFSI/ $Na_3Zr_2Si_2PO_{12}$	1.03×10^{-5} (25 °C)	–	–	[16]
PEO/NaTFSI/Na_3SbS_4	2.47×10^{-5} (25 °C) 3.72×10^{-5} (30 °C) 1.33×10^{-4} (45 °C) 3.08×10^{-4} (60 °C) 5.64×10^{-4} (70 °C)	0.49	345	This work

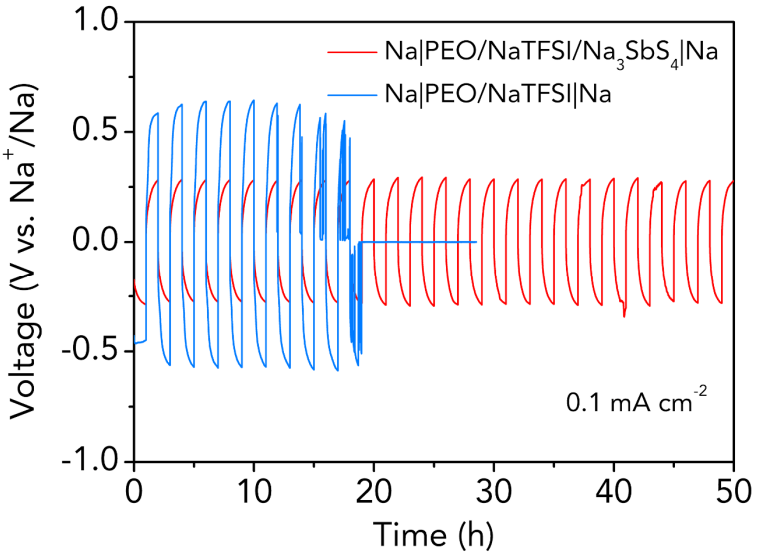

Figure S10. Voltage profiles of symmetric cells with PEO/NaTFSI electrolyte and PEO/NaTFSI/Na_3SbS_4 electrolyte at 0.1 mA cm^{-2} and 45 °C.

Table S3. Comparison on performance of the Na|Na symmetric cells in this work versus other reported Na|Na symmetric cells with polymer-based all-solid-state electrolytes.

Electrolyte	Current density (mA cm^{-2}) /overpotential (V)	Test temperature (°C)	Ref.
PEO/NaFNFSI	0.1/~0.09	80	[8]
PEO/CQDs/$NaClO_4$	0.05/~0.18, 0.1/~0.32	60	[9]
HMOP–PEO–NaTFSI	0.3/~0.8	65	[17]
PEGDMA–NaFSI–SPE	0.1/~0.6	60	[18]
PVDF/$NaCF_3SO_3$/SiO_2	0.2/~0.6	60	[19]
PEO/$Na_2Zn_2TeO_6$/NaTFSI	0.1/~0.4	80	[20]
PEO/NaTFSI/Na_3SbS_4	0.05/0.153, 0.1/0.504	45	This work

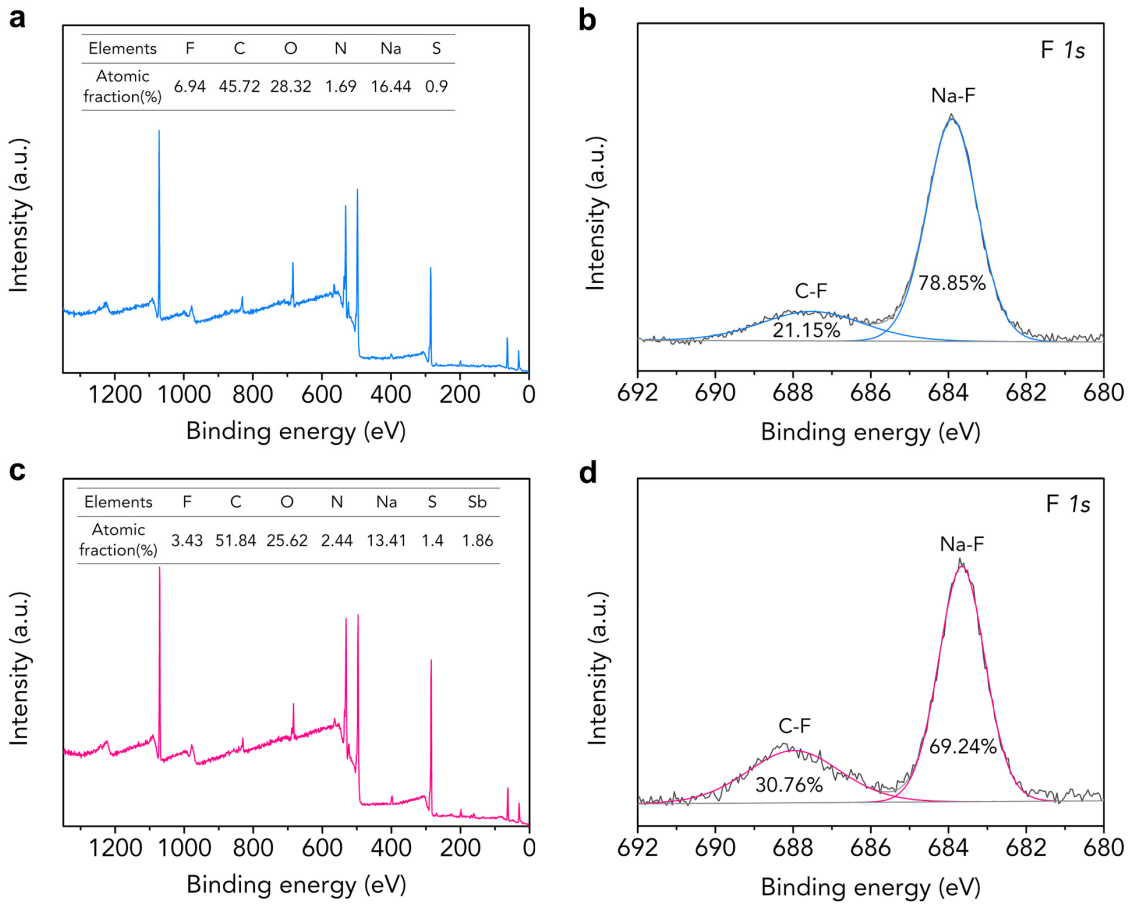

Figure S11. XPS survey and F 1s spectra of Na electrode after stripping/plating with different all-solid-state electrolytes. (a,b) PEO/NaTFSI electrolyte. (c,d) PEO/NaTFSI/Na_3SbS_4 electrolyte. Insets in (a) and (c): the corresponding atomic fraction of different elements.

The total ratio of F element on Na anode in the PEO/NaTFSI/Na_3SbS_4 electrolyte system (3.43 at%, Figure S11c) is lower than that in the PEO/NaTFSI electrolyte system (6.94 at%, Figure S11a). Moreover, the Na–F ratio among all the F-containing species in the former system (69.24%, Figure S11d) is lower than that in the latter system (78.85%, Figure S11b). Thus, we can conclude that the ratio of generated NaF among all the SEI species on Na electrode after stripping/plating with PEO/NaTFSI/Na_3SbS_4 electrolyte is lower than that with PEO/NaTFSI electrolyte.

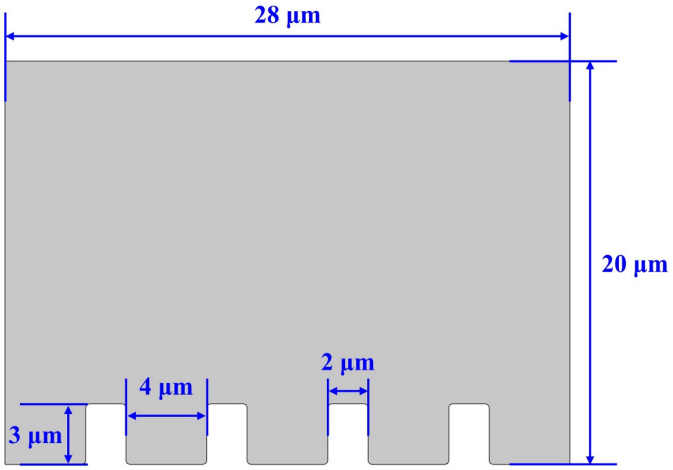

Figure S12. Geometry used in FEM simulation.

Table S4. FEM simulation parameters setting for Na deposition.

Parameters	PEO/NaTFSI	PEO/NaTFSI/Na_3SbS_4
Na^+ concentration (mol L^{-1})	2.5	2.5
Na^+ transference number	0.20	0.49
Na^+ diffusion coefficient (10^{-10} cm^2 s^{-1})	5	5
Exchange current density (mA cm^{-2})	0.5	0.5
Ionic conductivity (10^{-5} S cm^{-1})	4.19	13.3

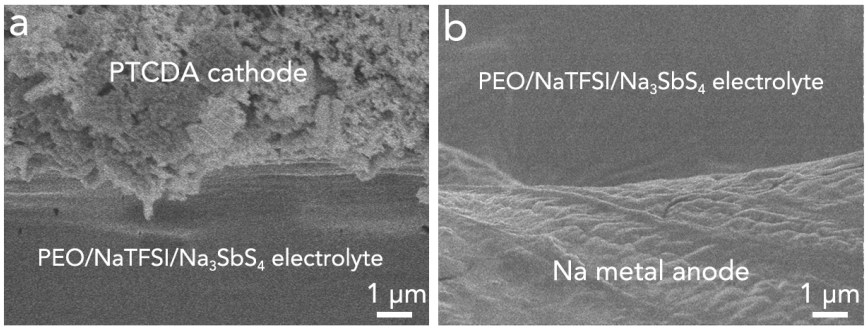

Figure S13. High-resolution SEM images of the interface between (a) PEO/NaTFSI/Na_3SbS_4 electrolyte and PTCDA cathode, (b) PEO/NaTFSI/Na_3SbS_4 electrolyte and Na metal anode.

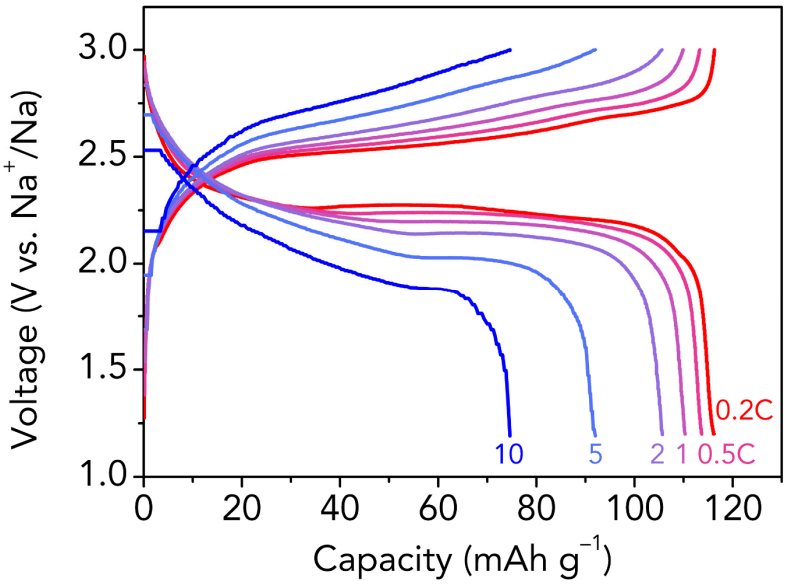

Figure S14. Discharge and charge profiles of the all-solid-state Na–PTCDA batteries with PEO/NaTFSI electrolyte at different rates (0.2, 0.5, 1, 2, 5, and 10 C) and 45 °C.

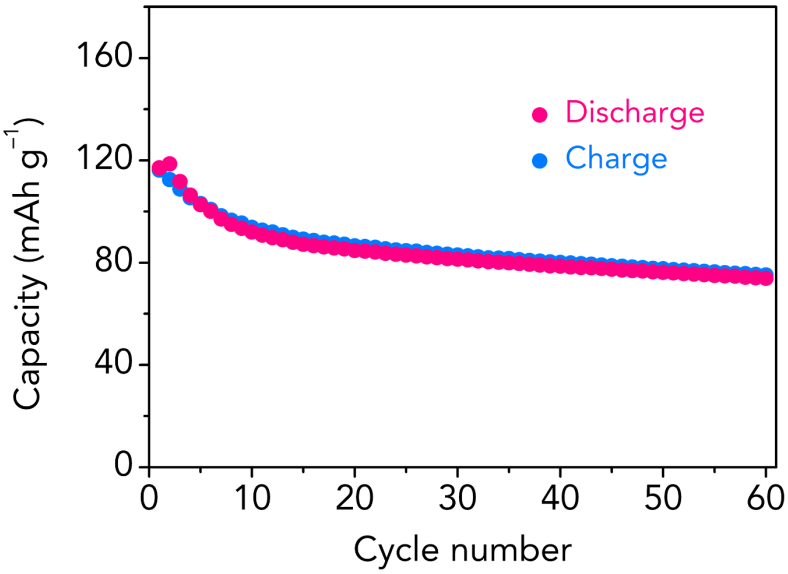

Figure S15. Cycling performance of Na–PTCDA batteries with 1M $NaPF_6$/diglyme electrolyte at 0.2 C and room temperature.

Table S5. Comparison on performance of the Na–PTCDA batteries in this work versus other reported Na batteries with polymer-based all-solid-state electrolytes (Here all the anodes are Na metals).

Electrolyte	Cathode	Rate performance [a)]	Cycling performance [b)]	Test temperature [c)]	Ref.
PEO/NaFNFSI	$NaCu_{1/9}Ni_{2/9}Fe_{1/3}Mn_{1/3}O_2$	89.7/2 C	~75/70%/150	80	[8]
PEO/CQDs/$NaClO_4$	$Na_3V_2(PO_4)_3$	56/8 C	89.4/88%/100	60	[9]
PEO/$NaClO_4$/$Na_3Zr_2Si_2PO_{12}$	$Na_2MnFe(CN)_6$	88/2 C	90.8/83%/300	60	[10]
HMOP–PEO–NaTFSI	$NaTi_2(PO_4)_3$	–	80/69.6%/~120	65	[17]
PVDF/$NaCF_3SO_3$/SiO_2	$Na_3V_2(PO_4)_3$	54/5 C	~88/86%/250	60	[19]
PEO/beta-alumina/$NaClO_4$	$Na_3V_2(PO_4)_3$	61.5/2 C	77.8/83.6%/100	60	[21]
PEO/TiO_2/$NaClO_4$	$Na_{2/3}Co_{2/3}Mn_{1/3}O_2$	–	45/~90%/25	60	[22]
PEO/NaTFSI/Na_3SbS_4	PTCDA	92/10 C	101/84%/200	45	This work

a) The values in this column represent capacity (mAh g^{-1}) and corresponding current rate, respectively.

b) The values in this column represent capacity (mAh g^{-1}) after cycles, capacity retention, and corresponding cycle number, respectively.

c) The unit of test temperature is °C.

References

[1] J. Wei, J. Wei, D. Lan, Z. He, H. Lu, Y. Cao and Z. Lu, CN 108163890 A, 2018.

[2] a) G. Kresse and J. Furthmüller, *Phys. Rev. B*, 1996, **54**, 11169−11186. b) P. E. Blöchl, *Phys. Rev. B*, 1994, **50**, 17953−17979.

[3] J. P. Perdew, K. Burke and M. Ernzerhof, *Phys. Rev. Lett.*, 1996, **77**, 3865−3868.

[4] X. Xu, Y. Liu, J.-Y. Hwang, O. O. Kapitanova, Z. Song, Y.-K. Sun, A. Matic and S. Xiong, *Adv. Energy Mater.*, 2020, **10**, 2002390.

[5] A. Arya and A. L. Sharma, *J. Solid State Electrochem.*, 2018, **22**, 2725−2745.

[6] X. Zhang, X. Wang, S. Liu, Z. Tao and J. Chen, *Nano Res.*, 2018, **11**, 6244−6251.

[7] Y. Lu, Y. Cai, Q. Zhang, L. Liu, Z. Niu and J. Chen, *Chem. Sci.*, 2019, **10**, 4306−4312.

[8] Q. Ma, J. Liu, X. Qi, X. Rong, Y. Shao, W. Feng, J. Nie, Y.-S. Hu, H. Li, X. Huang, L. Chen and Z. Zhou, *J. Mater. Chem. A*, 2017, **5**, 7738−7743.

[9] C. Ma, K. Dai, H. Hou, X. Ji, L. Chen, D. G. Ivey and W. Wei, *Adv. Sci.*, 2018, **5**, 1700996.

[10] X. Yu, L. Xue, J. B. Goodenough and A. Manthiram, *ACS Mater. Lett.*, 2019, **1**, 132−138.

[11] S. Chen, F. Feng, Y. Yin, H. Che, X.-Z. Liao and Z.-F. Ma, *J. Power Sources*, 2018, **399**, 363−371.

[12] Y. Zheng, Q. Pan, M. Clites, B. W. Byles, E. Pomerantseva and C. Y. Li, *Adv. Energy Mater.*, 2018, **8**, 1801885.

[13] H. K. Koduru, Y. G. Marinov, G. B. Hadjichristov and N. Scaramuzza, *Solid State Ionics*, 2019, **335**, 86−96.

[14] C. Sångeland, R. Younesi, J. Mindemark and D. Brandell, *Energy Storage Mater.*, 2019, **19**, 31−38.

[15] Z. Ge, J. Li and J. Liu, *Ionics*, 2020, **26**, 1787−1795.

[16] K. Hiraoka, M. Kato, T. Kobayashi and S. Seki, *J. Phys. Chem. C*, 2020, **124**, 21948−21956.

[17] W. Zhou, H. Gao and J. B. Goodenough, *Adv. Energy Mater.*, 2016, **6**, 1501802.

[18] Y. Yao, Z. Wei, H. Wang, H. Huang, Y. Jiang, X. Wu, X. Yao, Z.-S. Wu and Y. Yu, *Adv. Energy Mater.*, 2020, **10**, 1903698.

[19] S. Bag, C. Zhou, S. Reid, S. Butler and V. Thangadurai, *J. Power Sources*, 2020, **454**, 227954.

[20] J.-F. Wu, Z.-Y. Yu, Q. Wang and X. Guo, *Energy Storage Mater.*, 2020, **24**, 467−471.

[21] Y. Yao, Z. Liu, X. Wang, J. Chen, X. Wang, D. Wang and Z. Mao, *J. Mater. Sci.*, 2021, **56**, 9951−9960.

[22] Y. L. Ni'mah, M.-Y. Cheng, J. H. Cheng, J. Rick and B.-J. Hwang, *J. Power Sources*, 2015, **278**, 375−381.